Li *et al. Ecological Processes* (2024) 13:35
https://doi.org/10.1186/s13717-024-00514-8

Ecological Processes

RESEARCH

Open Access

Ratio of photosynthetically active radiation to global solar radiation above forest canopy in complex terrain: measurements and analyses based on Qingyuan Ker Towers

Shuangtian Li[1,2,3,4], Qiaoling Yan[1,2,3], Tian Gao[1,2,3*], Xingchang Wang[3,5], Qingwei Wang[2], Fengyuan Yu[1,2,3], Deliang Lu[1,2,3], Huaqi Liu[1,2,3], Jinxin Zhang[1,2,3] and Jiaojun Zhu[1,2,3]

Abstract

Background Understanding of the ratio of photosynthetic photon flux density (Q_p) to global solar radiation (R_s) (Q_p/R_s) is crucial for applying R_s to ecology-related studies. Previous studies reported Q_p/R_s and its variations based on measurements from a single observatory tower, instead of multi-site-based measurements over complex terrains. This may neglect spatial heterogeneity in the terrain, creating a gap in an understanding of how terrain affects Q_p/R_s and how this effect interacts with meteorological factors.

Methods Here the Qingyuan Ker Towers (three towers in a valley with different terrains: T1, T2, and T3) were utilized to measure Q_p and R_s over mountainous forests of Northeast China. An airborne LiDAR system was used to generate a digital elevation model, and sky view factor of sectors (SVF_s) divided from the field of view of tower's pyranometer was calculated as a topographic factor to explain the variations of Q_p/R_s.

Results The results identified significant differences in Q_p/R_s of the three towers at both daily and half-hour scales, with larger differences on clear days than on overcast days. Q_p/R_s was positively correlated with SVF_s of T1 and T3, while this correlation was negative with that of T2. The effect of SVF_s on Q_p/R_s interacted with clearness index, water vapor pressure and solar zenith angle. Random forest-based importance assessment demonstrated that explanation (R^2) on Q_p/R_s was improved when SVF_s was included in the predictor variable set, indicating that incorporating terrain effects enhances the prediction accuracy of Q_p/R_s. The improvement in the R^2 values was more pronounced on clear days than on overcast days, suggesting that the effect of terrain on Q_p/R_s depended on sky conditions.

Conclusions All findings suggested that Q_p/R_s is affected by terrain, and integrating terrain information into existing Q_p/R_s models is a feasible solution to improve Q_p/R_s estimates in mountainous areas.

Keywords Photosynthetic photon flux density, Clearness index, Water vapor pressure, Solar zenith angle, Terrain, Sky view factor

*Correspondence:
Tian Gao
tiangao@iae.ac.cn
Full list of author information is available at the end of the article

Introduction

The solar radiation at the wavelength range of 400–700 nm, which can be absorbed by green plants to convert light energy into chemical energy in photosynthesis processes, is called photosynthetically active radiation (PAR) (Mayer et al. 2002; McCree 1972). PAR is quantified using either photon term in μmol m^{-2} s^{-1} or energy term in W m^{-2}. The former is used in this study and denoted by Q_p. Q_p is an indispensable input variable for modelling photosynthesis and primary productivity of terrestrial vegetation (Alados et al. 1996; Jacovides et al. 2007; Qin et al. 2018), and plays an important role in a variety of applications in ecology, forestry and agriculture (Alados et al. 1996; Akitsu et al. 2022; Proutsos et al. 2019). Therefore, accurate estimation of Q_p is fundamental to understanding the exchange of CO_2 between the atmosphere and ecosystems. Unfortunately, Q_p is measured not by most radiation stations particularly for a long term in the past due to problems with accuracy and availability of quantum sensors (Akitsu et al. 2017; Mizoguchi et al. 2010; Wang et al. 2015a, b). Alternatively, Q_p is often converted from global solar radiation (R_s; W m^{-2}) through a certain ratio of Q_p to R_s (Q_p/R_s), since R_s is more routinely monitored in more meteorological stations with a high better availability and accuracy (Akitsu et al. 2015).

Q_p/R_s values have been reported worldwide. The general idea of previous researches is to reveal how meteorological factors (e.g., clearness index, sky clearness, sky brightness, solar zenith angle and water vapor) affect Q_p/R_s (Foyo-Moreno et al. 2017; Wang et al. 2014; Yamashita and Yoshimura 2019; Zhu et al. 2015). For instance, Alados et al. (1996) developed different empirical models relating Q_p/R_s to sky condition, solar zenith angle and dew point temperature. Jacovides et al. (2007) suggested that the variability of Q_p/R_s was closely associated with local cloud conditions and aerosol content. Although some work has been conducted, yet few studies have addressed the interaction among meteorological factors especially in different sky conditions. For example, a lower clearness index is often accompanied by a higher water vapor pressure. It is unclear how their linkages affect their relationship to Q_p/R_s, and further affect Q_p/R_s modeling.

Q_p/R_s over a complex terrain may be altered by reflected radiation from the surrounding terrain. Generally, incident solar radiation at a point on the surface of complex terrain is the sum of three components: direct radiation from the sun to ground surface, diffuse radiation from the sky hemisphere, and reflected radiation from the hemisphere obstructed by surrounding terrain (Allen et al. 2006; Dubayah and Rich 1995). Pyranometers are commonly deployed in open areas without obstructions to measure solar radiation (Akitsu et al. 2017). In mountainous regions, however, complex terrain may alter the field of view (FOV) of pyranometers, resulting in reflected radiation from the surrounding mountains entering the pyranometer sensors (Li et al. 2016; Zhang et al. 2019). Different medias have different properties of absorption and reflection at different wavelength bands, resulting in differences in reflected Q_p and reflected R_s from both the unobstructed sky and surrounding terrain (Li et al. 2016; Zhang et al. 2019), which can further alter the Q_p/R_s entering FOV of pyranometers. Therefore, uncertainties in the measurements of the Q_p/R_s may generate if the topographical effect is not adequately considered (Wang et al. 2005, 2006). In addition, the redistribution of incident solar radiation dominated by terrain complicatedly interacts with solar position and sky conditions (Aguilar et al. 2010; Dubayah and Rich 1995; Zhang et al. 2019). For example, since diffuse solar radiation is lower in intensity and distributed more uniformly than direct solar radiation, the effect of terrain on the redistribution of incident solar radiation is less pronounced on cloudy days dominated by diffuse radiation than on clear days dominated by direct radiation. Previous studies have revealed that the solar radiation and its components over complex terrain have great spatio-temporal variation and heterogeneity due to the influence of terrain shading and clouds (Bosch et al. 2009; Wang et al. 2006; Zhang et al. 2019). However, understanding the effect of terrain on the Q_p/R_s is hampered by lacking multi-location-based measurement in complex terrain, which resulted in a gap in an understanding of how terrain influence Q_p/R_s, and how this influence interacts with sun position and sky conditions.

Here, we hypothesize that there is a difference in the R_s and Q_p received from the sky and reflected from the surrounding terrain within the FOV of pyranometer, which further alters Q_p/R_s above forest canopy. To validate the hypothesis, we measured Q_p and R_s at three observation sites with different terrain features in a valley, and compared the difference in Q_p/R_s of the three observation sites. We also analyzed how the interactive influence of terrain and meteorological factors on Q_p/R_s, and assessed the importance of both terrain and meteorological factors in explaining the variations in Q_p/R_s. This study provides new insights into the accurate modeling of Q_p/R_s in complex terrains.

Materials and methods

Study site and radiation measurements

The experimental site was located in the Qingyuan Forest CERN, National Observation and Research Station, Liaoning Province, Northeast China (124°54′E, 41°51′N, 500–1100 m a.s.l.). The area belongs to a temperate

continental monsoon climate with a mean annual air temperature of 4.3 °C and mean annual precipitation of 758 mm during 2010–2021.

The Qingyuan Ker Towers were comprised of three 50-m-high eddy covariance towers erected on the sidewalls of the valley, running from southwest to northeast (Fig. 1). Each tower was independently located in a subwatershed covered with mixed broadleaved forest (T1; *Acer mono*, *Fraxinus rhynchophylla*, *Juglans mandshurica*, and *Quercus mongolica*, etc.), Mongolian oak forest (T2; *Quercus mongolica*) forest, and larch (*Larix kaempferi*) plantation forest (T3), respectively (Gao et al. 2020).

The radiation sensors of the three towers were horizontally installed on 2 m south-facing arms at 46.5 m above the ground. R_s was measured by means of CNR4 pyranometers (Kipp & Zonen, Delft, Netherlands) which were calibrated by factory before delivery. Q_p was measured using PQS1 quantum sensors (Kipp & Zonen, Delft, Netherlands). To eliminate systematic errors among the quantum sensors of the three towers, we used a quantum sensor that was parallel with the routine quantum sensors at the original position (distance less than 1 m) and measured Q_p for reference. The relationships of measured Q_p between the reference sensor and the routine sensors of the three towers were fitted (T1: $y = 1.1532x$, $R^2 = 0.998$, $P < 0.001$; T2: $y = 1.0554x$, $R^2 = 1$, $P < 0.001$; T3: $y = 1.0427x$, $R^2 = 0.995$, $P < 0.001$). The radiation data used for fitting covered a range of radiation gradients and met requirements for radiometric calibration. The quantum sensors were multiplied by the corresponding correction coefficient to correct the systematic errors, respectively. Air temperature and relative humidity of the three towers were measured by the HMP155A sensors (Vaisala, Helsinki, Finland) installed 46.5 m above the ground. The sensors sampled every 5 s, and half-hourly averages of radiation and environmental factors were collected through CR1000X data-loggers and CR6 data-loggers, respectively, from January 2020 to December 2020.

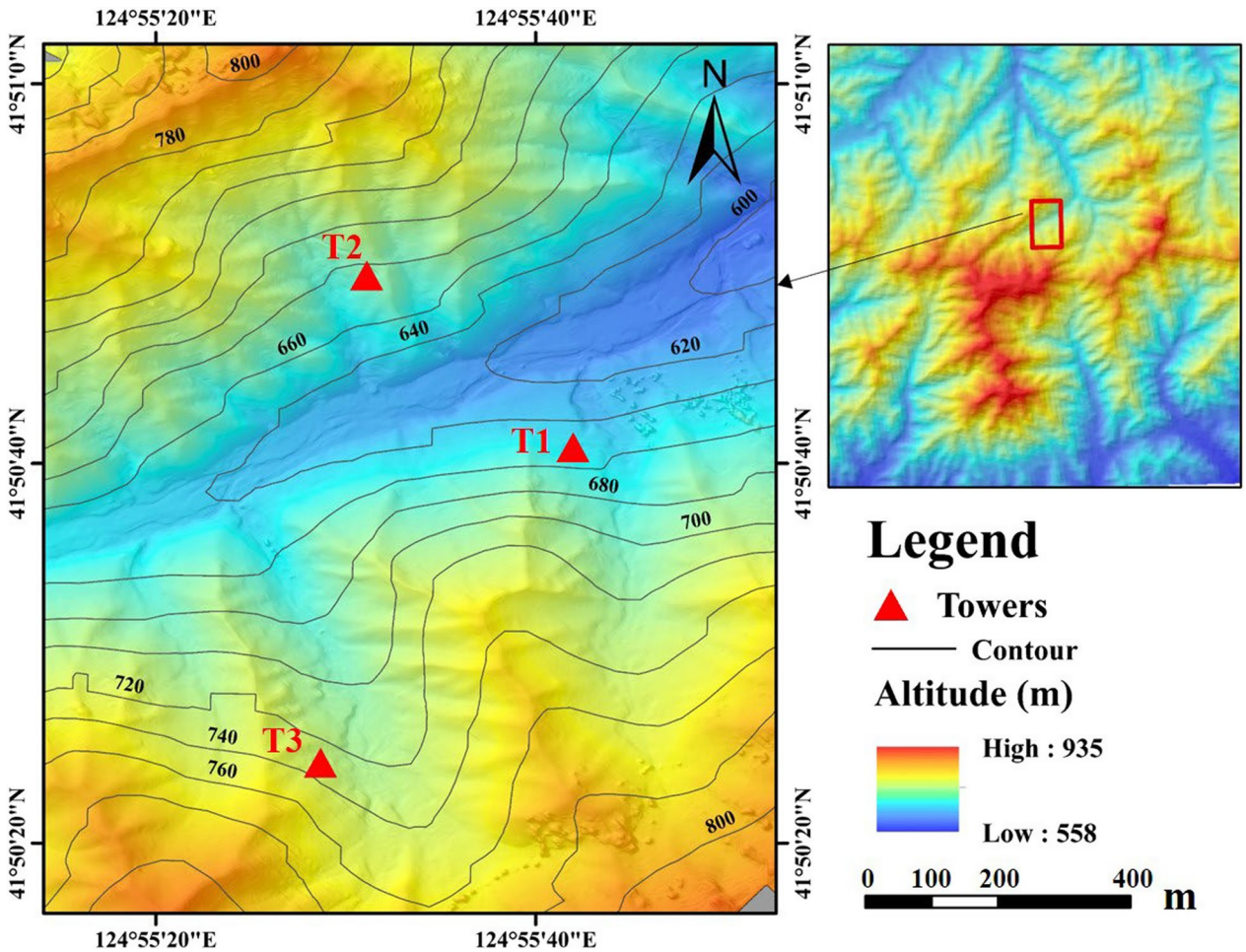

Fig. 1 Spatial distribution of the three towers. T1: Tower 1; T2: Tower 2; T3: Tower 3

Data process

Data preprocessing

Gaps in R_s and Q_p of the three towers were filled using measurements from the adjacent towers (e.g., gaps in T1 were filled with measurements from T2). Daily R_s and Q_p values were calculated by summing the half-hourly R_s and Q_p values recorded for daytime when $Q_p > 1$ μmol m^{-2} s^{-1}. The percentage of missing R_s data were 2.6%, 1.7%, and 3.6% for T1, T2 and T3, respectively. The percentage of missing Q_p data were 0.6%, 0.3%, and 1.4% for T1, T2 and T3, respectively. All gap filling data of R_s and Q_p were used to calculate the values of annual or monthly radiation but not to perform any statistical analysis (e.g., correlation analysis).

Prior to analyzing the half-hourly Q_p/R_s and its influencing factors, it is necessary to perform quality control on half-hourly Q_p/R_s to remove erroneous data. Q_p/R_s value outside the range from 1.3 μmol J^{-1} to 2.8 μmol J^{-1} were excluded for analysis (Proutsos et al. 2019; Wang et al. 2014). To eliminate the problem caused by cosine response, data with solar zenith angle greater than 78° were also excluded (Akitsu et al. 2015; Proutsos et al. 2019). Additionally, data were eliminated when R_s values exceeded the extraterrestrial shortwave radiation, as well as when both of R_s and the extraterrestrial shortwave radiation are less than 5 W m^{-2}.

Clearness index (Kt) and water vapor pressure (e)

Clearness index (K_t) refers to the ratio of the global solar radiation incident on the horizontal plane to the extraterrestrial global solar radiation R_a (W m^{-2}) (Tsubo and Walker 2005), which represents the cloud and aerosol content in the atmosphere (Jacovides et al. 2007). R_a is determined as follows (Ham 2005):

$$R_a = G_{sc}(1 + 0.033\,(\cos\,(2\pi J/365)))\cos\theta \quad (1)$$

where G_{sc} is the solar constant (1367 W m^{-2}); J is the calendar day that counts from January 1; θ is the solar zenith angle.

According to half-hourly K_t, the sky condition was classified: $K_t \leq 0.3$, overcast day; $0.3 < K_t < 0.7$, partially cloudy days; $K_t \geq 0.7$, clear days (Yu et al. 2015). According to the grading standards of K_t, overcast days, partially cloudy days and clear days of the three towers accounted for 24.1 ± 1.2%, 44.8 ± 0.5%, and 31.2 ± 1.4%, respectively (data not shown).

Water vapor pressure (e) is used to represent the water vapor content in the atmosphere (Papaioannou et al. 1996). We directly used the half-hourly e collected by the data-logger according to air temperature and relative humidity (Tetens 1930).

Solar zenith angle (cosθ)

The cosine value of the solar zenith angle (cosθ), which is used to relate the path length of solar radiation passing through the atmosphere (Allen et al. 2006; Bosch et al. 2009). cosθ is calculated as following equation (Ham 2005):

$$\cos\theta = \sin\Phi\sin\delta + \cos\Phi\cos\delta\cos\,(15(t - t_0)) \quad (2)$$

where Φ is the latitude of the location; t is time; δ and t_0 are the solar declination angle and the solar time, respectively, given by Campbell et al. (1998):

$$\begin{aligned}\sin\delta\ =&0.39785\,\sin\,(278.97 + 0.9856J\\ &+1.9165\,\sin\,(356.6 + 0.9856J))\end{aligned} \quad (3)$$

$$t_0 = 12 - LC - ET \quad (4)$$

where LC is the longitude correction, to the east of the standard meridian of the local time zone: every 1° plus 4 min (1/15 h); west: every 1° minus 4 min. ET is the equation of time difference:

$$\begin{aligned}ET = \big(&-104.7\,\sin f\ + 596.2\,\sin 2f\\ &+ 4.3\,\sin 3f\ -\ 12.7\,\sin 4f\ -\ 429.3\,\cos f\\ &- 2.0\,\cos 2f\ +\ 19.3\cos 3f\big)/3600\end{aligned} \quad (5)$$

f is calculated as the following:

$$f = 279.575\ +\ 0.9856J \quad (6)$$

The cosine of the solar azimuth angle (cosψ) is used to determine the solar azimuth with respect to a specific location on Earth. The solar azimuth is defined based on the south meridian, where the counterclockwise direction is considered positive (0° to 180°), and the clockwise direction is considered negative (− 180° to 0°). cosψ is calculated as following equation (Ham 2005):

$$\cos\psi = (\cos\theta\sin\Phi - \sin\delta)/\cos\Phi\sin\theta \quad (7)$$

Sky view factor

Sky view factor (SVF), defined as a ratio of the unobstructed sky area to the total hemisphere sky area (Dubayah and Rich, 1995), was introduced to represent the sky visibility within the FOV of the observation location. We quantified the SVF by the following four steps. First, an airborne LiDAR system (Riegl VUX-1UAV) was used to generate a digital elevation model by point cloud from ground with a spatial resolution of 0.5 m (Chen et al. 2022). Second, we used the Solar Analyst in ESRI© ArcGIS 10.4 to generate a sky shed with a dimension of 200 × 200 grid, which spatially corresponds to the towers

(Zhang et al. 2019). Third, we partitioned the FOV of each tower's pyranometer into 36 sectors with an interval of 10°. Fourth, we employed color statistics analysis in Adobe Photoshop CS6 to calculate the numbers of pixels representing the terrain surface and sky, respectively. The ratio of sky coverage pixels to the total number of pixels within each sector was calculated and denoted as SVF_s.

Statistical analysis

One-way ANOVA was used to assess the differences in Q_p/R_s of the three towers at half-hourly and daily scales and under different sky conditions. Further, we compared the differences in Q_p/R_s of the three towers on typical overcast and clear days. Considering the influence of atmospheric water vapor content on Q_p/R_s, we selected several typical overcast and clear days in the dry season and the wet season respectively to compare the differences in Q_p/R_s. Specifically, we first calculated the differences in Q_p/R_s between each pair of towers on typical overcast and clear days in the dry and wet seasons, and since we are concerned with the magnitude of the differences in Q_p/R_s, we took the absolute values of these differences. Then we used the *T*-test to test the differences in Q_p/R_s between each pair of towers on typical overcast and clear days in both the dry and wet seasons. One-way ANOVA and *T*-test were performed using the "stats" R package.

Pearson's correlation coefficient (r) was introduced to examine the effect of K_t, e, $\cos\theta$ and SVF_s on Q_p/R_s in different sky conditions. Considering that the potential correlation among variables may affect the relationship analysis, we conducted a partial correlation analysis to exclude the mutual influence of variables. By controlling the influence of K_t, e, $\cos\theta$ and SVF_s on Q_p/R_s respectively, the relationship between other variables and Q_p/R_s was analyzed. To distinguish two types of correlation analysis, correlation analysis without controlling the influencing factors was expressed as zero-order correlation (Li et al. 2020). Correlation and partial correlation analysis were performed using the "Hmisc" R package and the "ppcor" R package, respectively.

A random forest (RF) model (Breiman 2001) was used to determine the contribution of terrain to the variation in Q_p/R_s and the importance for predicting Q_p/R_s. RF models are highly interpretable and non-parametric, and are suitable for constructing nonlinear relationships between Q_p/R_s and both meteorological and topographic factors (Breiman 2001). The number of regression trees (*ntree*) per group was set to 300, and the number of variables (*mtry*) per node building the regression tree was set to 2. Four datasets were generated (the whole year and the three types of sky conditions). Each dataset contained two groups of variables: one group included K_t, e and $\cos\theta$; the other included K_t, e, $\cos\theta$ and SVF_s. We assessed the variable importance in predicting Q_p/R_s using the mean square error (MSE) and the explained percentage of variance (R^2). These analyses and the significance tests of variables were performed using the "randomForest" R package and the "rfPermute" R package, respectively.

Results

Variation in daily and half-hourly Q_p/R_s

Temporal variation in daily Qp/Rs

Daily Q_p and R_s of the three towers presented a generally similar seasonal pattern (Fig. 2a, b), showing an increase from winter (16.953 ± 0.538 mol m^{-2} d^{-1} for Q_p and 9.105 ± 0.464 MJ m^{-2} for R_s; standard deviation was calculated from the values of the three towers and thereinafter) to summer (42.615 ± 0.578 mol m^{-2} d^{-1} for Q_p and 19.705 ± 0.246 MJ m^{-2} for R_s). The annual averaged Q_p and R_s values of the three towers were 29.499 ± 0.182 mol m^{-2} d^{-1} and 14.447 ± 0.235 MJ m^{-2}, respectively. Daily Q_p/R_s also presented seasonality (Fig. 2c). The Q_p/R_s was higher in summer (2.186 ± 0.015 mol MJ^{-1}) and lower in winter (1.910 ± 0.043 mol MJ^{-1}), with intermediate values observed in spring (2.049 ± 0.035 mol MJ^{-1}) and autumn (2.037 ± 0.006 mol MJ^{-1}) (Fig. 2c). The seasonality of Q_p/R_s generally showed a similar response to seasonal variation in water vapor pressure (e) (Fig. 2c, d). Although the seasonal variations of Q_p/R_s of the three towers were generally comparable, significant differences were observed in their daily Q_p/R_s ($F = 5.19$, $P < 0.01$; Table 1).

Diurnal variation in half-hourly Qp/Rs

Q_p/R_s of T1 and T2 showed a similar diurnal variation during the growing season with remarkable fluctuations at near sunrise and sunset, as well as showed a slight increase at noon (Fig. 3a–g). Differently, the diurnal variation in Q_p/R_s of T3 increased in April ($slope = 0.022$, $P < 0.001$) and May ($slope = 0.008$, $P < 0.001$), with lower Q_p/R_s values at sunrise and higher Q_p/R_s values at sunset (Fig. 3a, b). The diurnal variations in Q_p/R_s of T3 generally exhibited a U-shaped pattern from June to October (Fig. 3c–g).

Figure 4 showed diurnal variations of Q_p/R_s on typical clear and overcast days in the peak growing season (additional information for other months can be found in Additional file 1: Figs. S1, S2). The diurnal variation of Q_p/R_s differed between clear and overcast days (Fig. 4, Additional file 1: Figs. S1, S2). Significant differences in the half-hourly Q_p/R_s were observed among the three

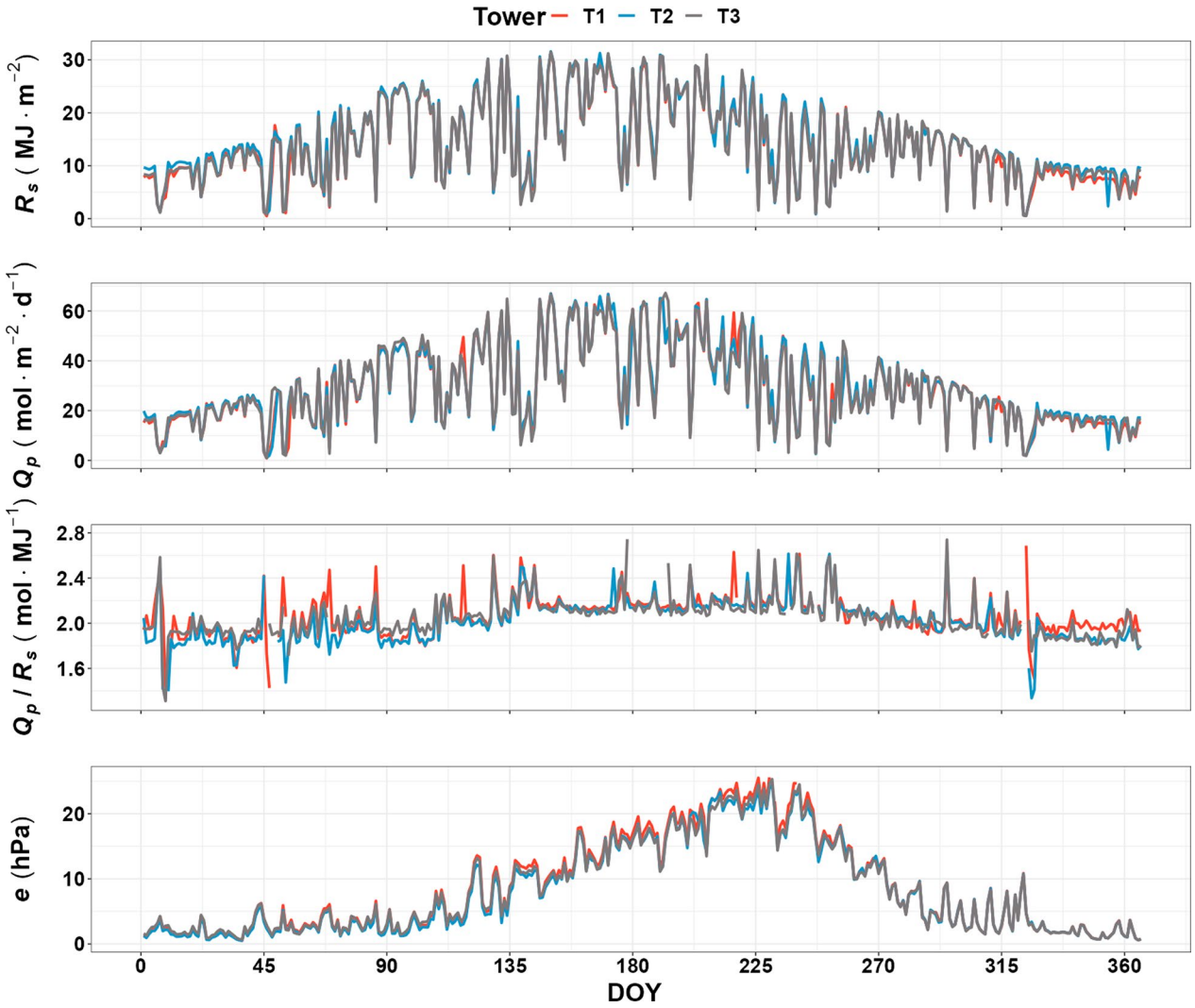

Fig. 2 Seasonal variation in R_s (**a**), Q_p (**b**), Q_p/R_s (**c**), and water vapor pressure e (**d**). T1: Tower 1; T2: Tower 2; T3: Tower 3

Table 1 Comparison of Q_p/R_s monitored by the three towers

Data type	Sky condition	*DF*	*F* value	*P*
Daily Q_p/R_s	All	2	5.19	0.006
Half-hourly Q_p/R_s	All	2	32.92	0.000
	Overcast days	2	10.3	0.000
	Partially cloudy days	2	8.802	0.000
	Clear days	2	8.9	0.000

For the daily Q_p/R_s, it is difficult to categorize the exact sky conditions and to ensure sufficient data availability for statistical analysis in a given sky condition, so we only compare the differences in Q_p/R_s among the three towers on a half-hour scale in different sky conditions

towers in the different sky conditions ($P<0.001$; Table 1). The significantly higher difference in the half-hourly Q_p/R_s was exhibited on clear days than on overcast days (Fig. 5).

Dependence of meteorological factors on Q_p/R_s

Dependence of Qp/Rs on Kt

Q_p/R_s of the three towers was negatively correlated with K_t in the whole year (the zero-order correlation, Pearson's $r=-0.636\pm0.039$, $P<0.001$) (Fig. 6a–c). Correlations between Q_p/R_s and K_t was significant (r were -0.665 ± 0.033, -0.570 ± 0.040 and -0.625 ± 0.023, respectively, $P<0.001$), even though effects of cosθ, e, and SVF$_s$ were excluded (Fig. 6a–c). The correlations between Q_p/R_s and K_t were -0.457 ± 0.096 on overcast days, -0.264 ± 0.032 on partially cloudy days and -0.392 ± 0.067 on clear days, respectively (Fig. 6d–l). Correlations between Q_p/R_s and K_t remained significant and stable when the effects of cosθ, e, and SVF$_s$ on Q_p/R_s were excluded (except on clear days) (Fig. 6d–i).

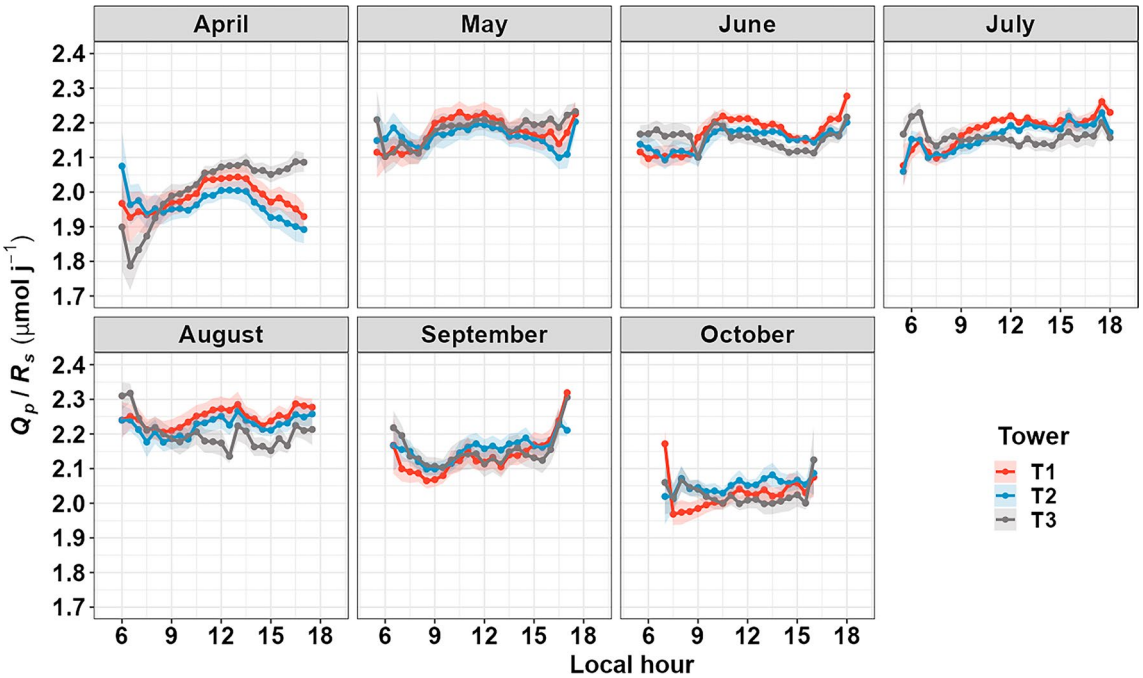

Fig. 3 Diurnal variations of the half-hourly Q_p/R_s during the growing season. Shaded regions represent the standard error of the half-hourly Q_p/R_s average. T1: Tower 1; T2: Tower 2; T3: Tower 3. The diurnal variation of Q_p/R_s in the non-growing season may fluctuate greatly due to the interference of snowfall and snow cover on the mountain surface. Here we only showed the diurnal variations of Q_p/R_s in the growing season (from April to October)

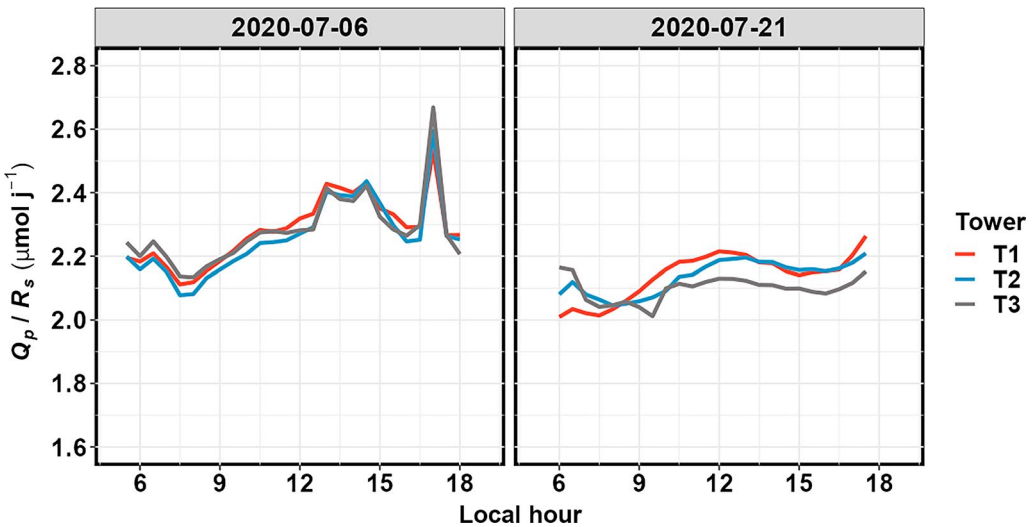

Fig. 4 Diurnal variations of Q_p/R_s on typical overcast and clear days. 6 July 2020 (**a**) and 21 July 2020 (**b**) were considered as typical overcast and clear days, respectively. T1: Tower 1; T2: Tower 2; T3: Tower 3

Dependence of Qp/Rs on e

Q_p/R_s of the three towers was positively correlated with e in the whole year ($r = 0.559 \pm 0.046$, $P < 0.001$) (Fig. 6a–c). The correlations were weakened (r were 0.467 ± 0.068, 0.513 ± 0.046 and 0.538 ± 0.066, respectively), when effects of K_t, $\cos\theta$, and SVF_s were excluded (Fig. 6a–c). The correlations also depended on sky conditions. The correlations were weaker on overcast days ($r = 0.350 \pm 0.057$, $P < 0.001$) than on partly cloudy ($r = 0.589 \pm 0.092$, $P < 0.001$) and clear

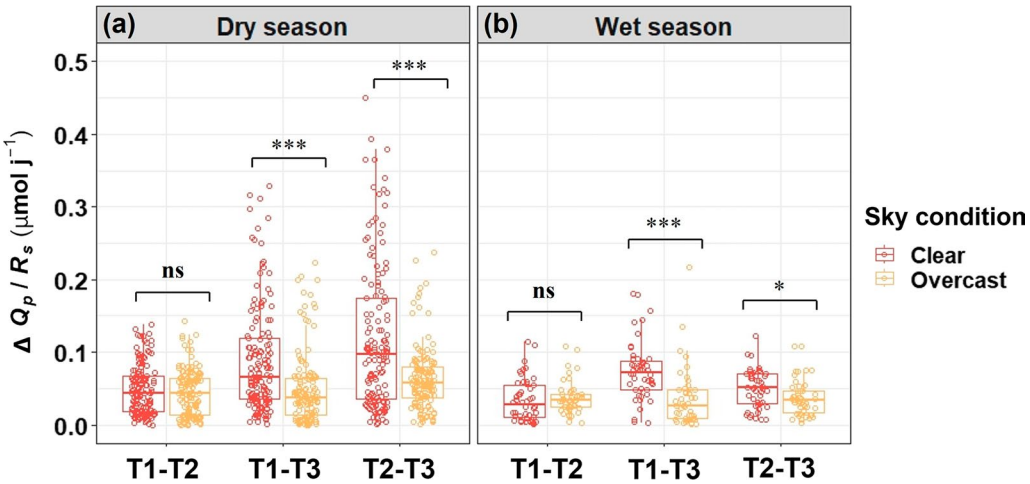

Fig. 5 Comparison of the differences in Q_p/R_s of the three towers on typical overcast and clear days in dry (**a**) and wet (**b**) seasons. Significance levels are: *$P<0.05$, **$P<0.01$, and ***$P<0.001$. T1: Tower 1; T2: Tower 2; T3: Tower 3

days ($r=0.756\pm0.075$, $P<0.001$) (Fig. 6d–l). For a given sky condition, the correlations of Q_p/R_s and e were still significant when the effects of the other factors were excluded (Fig. 6d–l). Differently, the correlations decreased when the effect of cosθ was removed (r were 0.322 ± 0.056 on overcast days, 0.516 ± 0.106 on partially cloudy days and 0.612 ± 0.094 on clear days; $P<0.001$) (Fig. 6d–l).

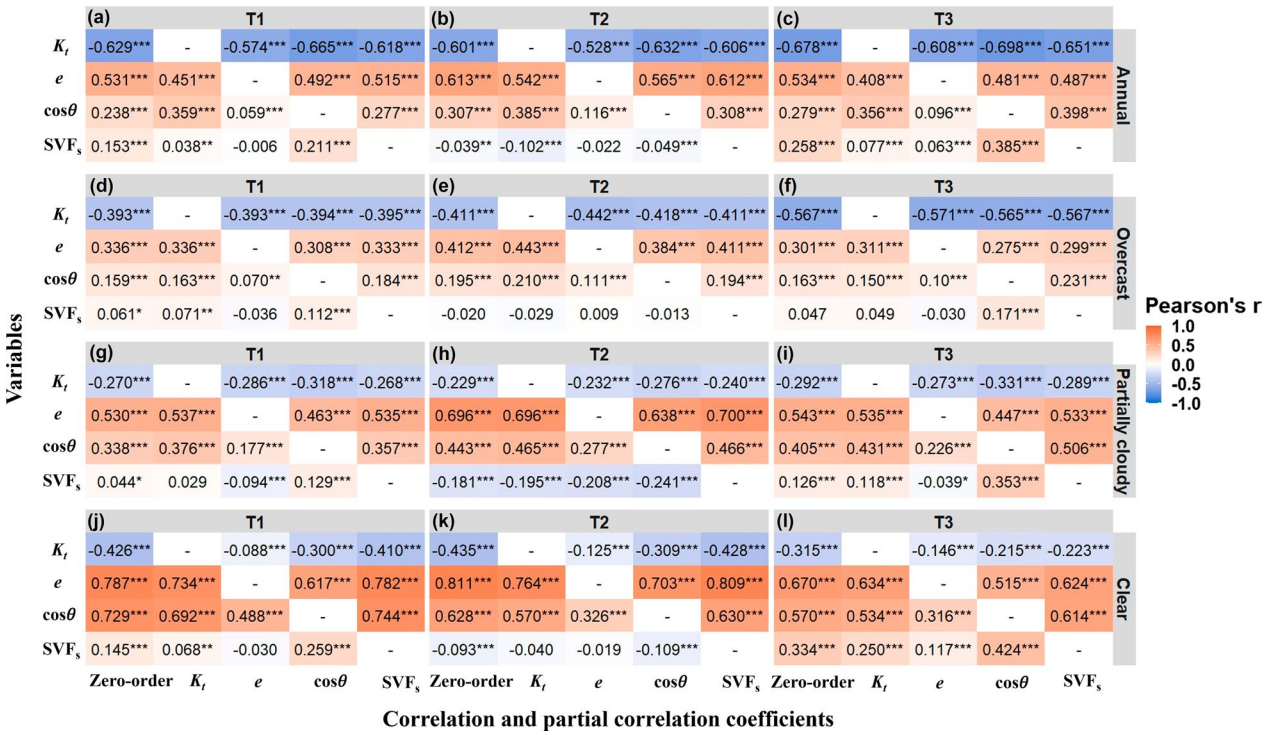

Fig. 6 Pearson correlations (zero-order correlation) and partial correlations between the half-hourly Q_p/R_s (μmol J^{-1}) values and the four variables (i.e., clearness index, cosine values of the solar zenith angle (cosθ), water vapor pressure, and sky view factor of sectors (SVF$_s$) of the three towers for the whole year, overcast days, partially cloudy days, and clear days. Significance levels are: *$P<0.05$, **$P<0.01$, and ***$P<0.001$. T1: Tower 1; T2: Tower 2; T3: Tower 3

Dependence of Qp/Rs on solar zenith angle

Q_p/R_s of the three towers was positively correlated with cosθ in the whole year ($r = 0.274 \pm 0.035$, $P < 0.001$) (Fig. 6a–c). The correlations were significant when effects of K_t, e and SVF_s were excluded, respectively (Fig. 6a–c). The correlations between cosθ and Q_p/R_s were observed to increase along a K_t gradient (r were 0.172 ± 0.020 on overcast days, 0.395 ± 0.053 on partly cloudy days, and 0.643 ± 0.080 on clear days; $P < 0.001$) (Fig. 6d–l). When effect of K_t was excluded, the correlations between Q_p/R_s and cosθ increased on partially cloudy days ($r = 0.424 \pm 0.045$, $P < 0.001$) while decreased on clear days ($r = 0.599 \pm 0.083$, $P < 0.001$) (Fig. 6d–l). The correlations did not change on overcast days ($r = 0.174 \pm 0.032$, $P < 0.001$). The effect of cosθ on Q_p/R_s was significantly weakened when effect of e was excluded (r were 0.095 ± 0.022 on overcast days, 0.227 ± 0.050 on partially cloudy days, and 0.377 ± 0.097 on clear days; $P < 0.001$), but was slightly enhanced when effect of SVF_s was excluded (r were 0.203 ± 0.024 for overcast days, 0.443 ± 0.077 for partially cloudy days, and 0.663 ± 0.071 for clear days, respectively; $P < 0.001$) (Fig. 6d–l).

Dependence of Q_p/R_s on SVF_s

The azimuthal variations of sky view factor of sectors

SVF_s of the pyranometers of the three towers showed different variation trends at − 180° to 180° azimuth (Fig. 7a–c). SVF_s of T1 showed a comparable W-shaped variation trend at − 180° to 180° azimuth (Fig. 7a). The variation trend of SVF_s of T2 was different from that of T1, showing an M-shaped variation trend at − 180° to 180° azimuth (Fig. 7b). The variation trend of SVF_s of T3 was similar to that of T1 (except − 180° to − 80° azimuth), showing a roughly symmetrical V-shaped variation trend at − 180° to 180° azimuth (Fig. 7c).

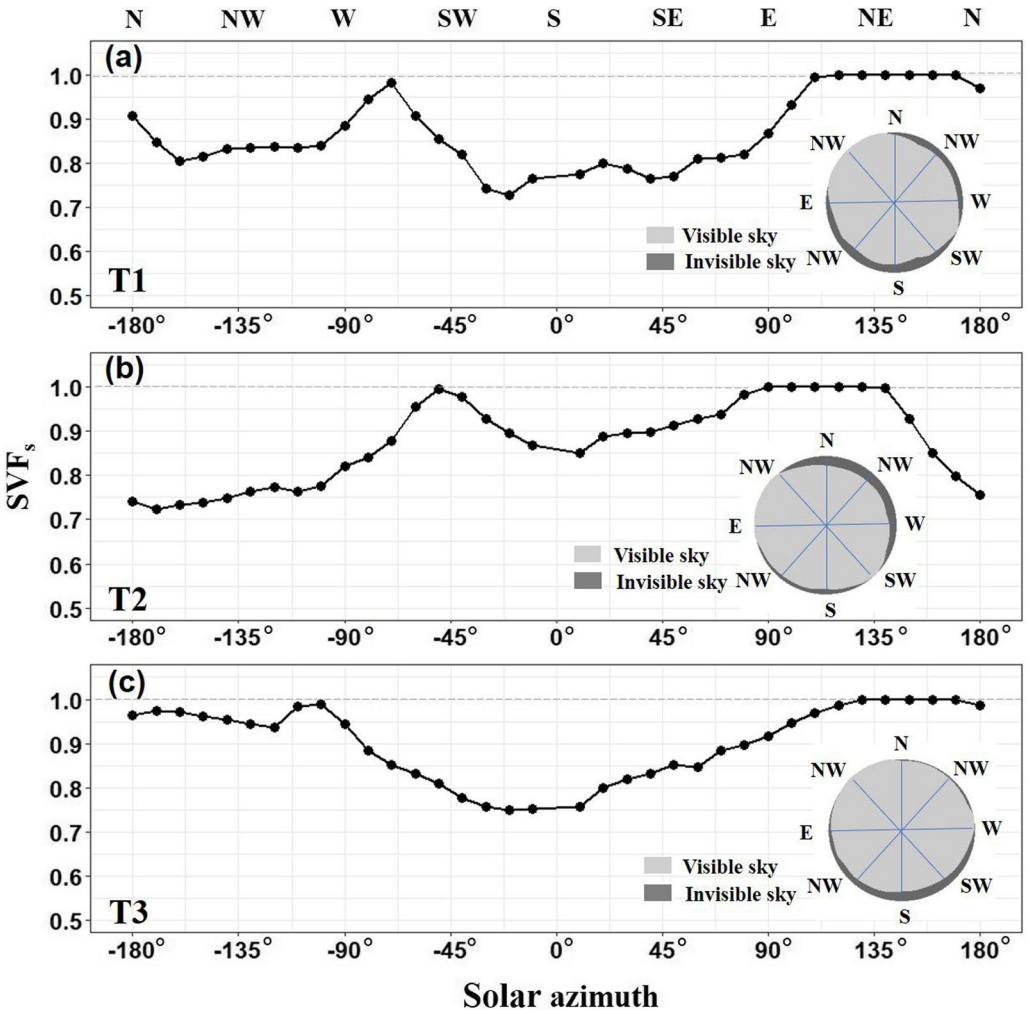

Fig. 7 The azimuthal variations of sky view factor of sectors (SVF_s) of the pyranometers of the three towers at − 180° to 180° azimuth. The dashed gray line indicates that the value of SVF_s is 1. T1: Tower 1; T2: Tower 2; T3: Tower 3

Dependence of Qp/Rs on SVF$_s$

SVF$_s$ were positively correlated with Q_p/R_s of T1 ($r=0.153$, $P<0.001$) and T3 ($r=0.258$, $P<0.001$), and were weakly and negatively correlated with Q_p/R_s of T2 ($r=-0.039$, $P<0.001$) in the whole year (Fig. 6a–c). Except for T1, no correlation between SVF$_s$ and Q_p/R_s was found on overcast days (Fig. 6d–f). SVF$_s$ were positively correlated with Q_p/R_s of T1 and T3 and were negatively correlated with Q_p/R_s of T2 on partially cloudy and clear days (Fig. 6g–l). The relationship between SVF$_s$ and Q_p/R_s was influenced, to some extent, by the interaction between SVF$_s$ and meteorological factors in different sky conditions (Fig. 6g–l). When the effect of K_t or e was excluded, the correlations between Q_p/R_s and SVF$_s$ were weakened and partially insignificant on partially cloudy and clear days (Fig. 6g–l). When the effect of cosθ was excluded, differently, correlations were significantly enhanced on partially cloudy days ($r=0.129$ for T1, -0.241 for T2, 0.353 for T3) and clear days ($r=0.259$ for T1, -0.109 for T2, 0.424 for T3) (Fig. 6g–l). In summary, correlations between SVF$_s$ and Q_p/R_s were found and were influenced by meteorological factors.

Importance assessment of variables

Including SVF$_s$ as an input variable of RF model can improve the predictive performance of Q_p/R_s. For the whole year, the R^2 value was improved by 5.04%, 3.65% and 7.36% for T1, T2 and T3, respectively, when including SVF$_s$ as the input variable (Fig. 8). For different sky conditions, the improvements in R^2 values were greater on clear and partially cloudy days than on overcast days (Fig. 8). For example, when SVF$_s$ was included, the R^2 values increased by 16.07% for T1, 8.95% for T2, and 20.79% for T3 on partially cloudy days, while increased by 2.84% for T1, 3.56% for T2, and 1.93% for T3 on overcast days (Fig. 8).

The variable importance varied depending on sky conditions. In non-SVF$_s$ groups, K_t was the most important, followed by e and cosθ in the whole year (Fig. 8). Along a K_t gradient (from clear days to overcast days), the importance of cosθ and e gradually increased (Fig. 8). e was the most important factor driving Q_p/R_s on partially cloudy and clear days (Fig. 8).

The SVF$_s$ importance varied among the three towers in different sky conditions. SVF$_s$ of T3 explained more Q_p/R_s than that of T1 and T2 in the whole year (Fig. 8). SVF$_s$ explained more to the changes in Q_p/R_s on partially cloudy and clear days than that on overcast days (Fig. 8). Note that SVF$_s$ was the most important factor affecting Q_p/R_s of T3 on partially cloudy and clear days (Fig. 8).

Discussion

Analysis of daily and half-hourly Q_p/R_s

The seasonal patterns of daily Q_p/R_s were generally similar among the three towers. Daily Q_p/R_s values were higher in summer than in winter (Fig. 2c), which was consistent with results reported by Akitsu et al. (2015), Hu and Wang (2012), and Wang et al. (2014). One possible explanation for the seasonal variation is associated with a high-water vapor content in summer, which can strongly absorb near-infrared radiation, whereas its effect on PAR is weak (Fig. 2c and d) (Alados and Alados-Arboledas 1999; Jacovides et al. 2007; Li et al. 2010).

Significant differences in Q_p/R_s were observed among the three towers at both daily and half-hour scales, supporting the hypothesis that topography alters Q_p/R_s above forest canopy. Since meteorological conditions, such as sky clearness index, water vapor pressure and solar zenith angle, were nearly consistent among the three towers, the differences in Q_p/R_s induced by meteorological factors are expected to be excluded. Note that the differences in Q_p/R_s of the three towers were larger on clear days than on overcast days (Fig. 5). Clear sky is dominated by direct beam, while overcast sky is dominated by diffuse radiation. The effect of topography on direct solar beam is significantly greater than that on diffuse solar radiation (Whiteman et al. 1989). We therefore conjectured that the differences in Q_p/R_s among the three towers may be related to the differences in reflected solar radiation from the surrounding terrain that enters the field of view of pyranometer. The effect of terrain on Q_p/R_s is discussed in Section "Effect of topography".

Effect of meteorological factors

Q_p/R_s is closely related to sky conditions and atmospheric water vapor. Previous investigations identified that the effect of cloud attenuation on solar radiation at near-infrared band includes absorption and scatter, whereas the attenuation on solar radiation at PAR band mainly involves the scatter (Alados and Alados-Arboledas 1999; Jacovides et al. 2007). A decrease in K_t has a pronounced impact on solar radiation at near-infrared band, leading to an increase in Q_p/R_s (Foyo-Moreno et al. 2017; Proutsos et al. 2019; Yu et al. 2015). Another reason may be that a low K_t is often along with overcast days. A high content of water vapor absorbs more solar radiation at near-infrared band than at PAR band, resulting in a higher PAR fraction (Alados and Alados-Arboledas 1999; Jacovides et al. 2007). The effect of K_t on Q_p/R_s remained significant and consistent when the effect of other factors (except on clear days) was excluded, indicating that K_t independently plays a crucial role in affecting Q_p/R_s. Along a K_t gradient (from clear days to overcast days),

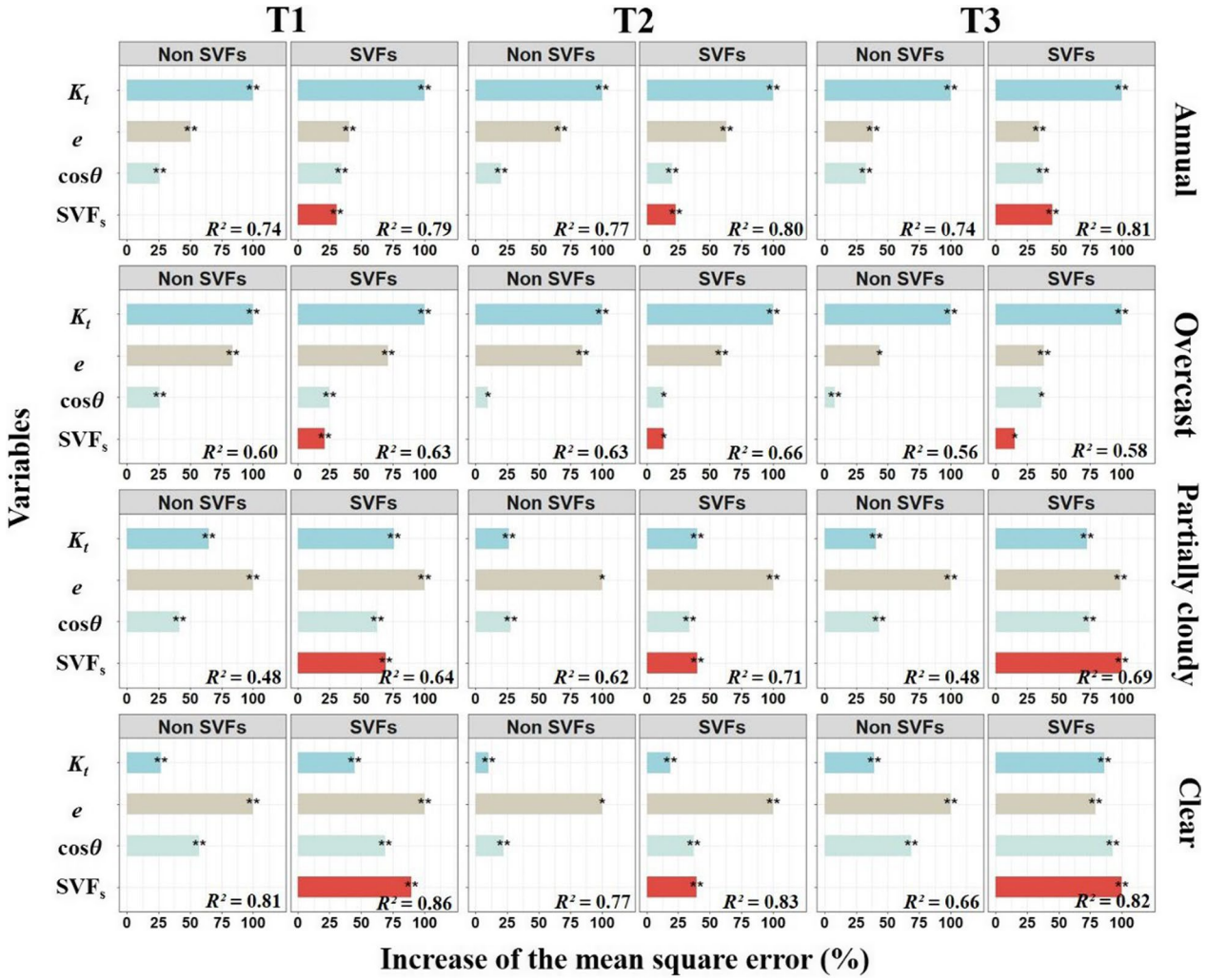

Fig. 8 Random forest model-based importance assessment of the two groups of variables on Q_p/R_s. Non-SVF_s groups include K_t, cosθ, and e, and SVFs groups include K_t, cosθ, e, and SVF_s. Increase of the mean square error is the percentage of variance explained by the two groups of variables for Q_p/R_s. The variable importance was normalized to a scale of 0 to 1. Significance levels are: $^*P < 0.05$, $^{**}P < 0.01$, and $^{***}P < 0.001$. T1: Tower 1; T2: Tower 2; T3: Tower 3

the effect of water vapor pressure on Q_p/R_s gradually weakens (Figs. 6d–l, 8), probably due to the difficulty of solar radiation penetrating the atmosphere in conditions of water vapor saturation (Proutsos et al. 2019). The reduced sensitivity of Q_p/R_s to water vapor pressure may introduce uncertainty in the estimation of Q_p/R_s on overcast days.

Q_p/R_s increased with cosθ. The medium in the atmosphere mainly absorbs the near-infrared band and scatters the PAR band. As the path length of solar radiation penetrates through the atmosphere decreases, light absorption at the near-infrared wavelength is stronger than light scattering at the PAR wavelength (Alados et al. 1996). As a result, solar radiation loses more at the near-infrared wavelength than at the PAR wavelength during the light transmission process, leading to an increase in Q_p/R_s (Jacovides et al. 2003). The effect of cosθ on Q_p/R_s was greater on clear days than on overcast days (Figs. 6d–l, 8). One possible explanation is that, on a clear day, solar radiation penetrating the atmosphere is mainly related to the penetrating path length, while other factors, such as clouds and water vapor in the atmosphere, can be negligible. On an overcast day, the transmission of solar radiation penetrating the atmosphere involves various factors and complex interaction effect. For example, the effect of cosθ on Q_p/R_s was significantly weakened when the effect of water vapor pressure was excluded (Fig. 6). This is probably due to an inherent link between the distance of radiation transmission and water vapor content. The variations in Q_p/R_s in response to changes in cosθ can be

partially attributed by water vapor pressure. Differently, we noticed that the effect of cosθ on Q_p/R_s was enhanced, when effect of SVF_s was excluded (Fig. 6), which may be due to the interaction between solar zenith angle and topography on solar radiation (further discussed in Section "Effect of topography").

Effect of topography

The two lines of evidence suggest that terrain affects Q_p/R_s, supporting our hypothesis. The surrounding terrain alters the field of view of the pyranometer, affecting the measured Q_p/R_s. Although three towers with different terrain features were used, fully comprehending the effect of terrain on Q_p/R_s is difficult. For statistical purposes, we partitioned the field of view of each observation into 36 sectors, which exhibits various terrain features (sky view factor in this case). The incident solar radiation azimuthally corresponding to a given sector may interact with terrain and generate special situation of reflection from the surrounding terrain, which can help us to understand the effect of terrain on Q_p/R_s.

The joint decreasing trends in sky view factor and Q_p/R_s may be related to a lower proportion of the sky in the sector that azimuthally corresponding to incidence solar radiation. The absorption of PAR is stronger by forested surface than by the sky. Therefore, the PAR that reflected from forested surface and then entering the pyranometer is lower than the PAR directly entering pyranometer from the sky, resulting in a decrease in Q_p/R_s of T1 and T3. Differently, the effects of SVF_s of the pyranometer of T2 on Q_p/R_s were contrary to that of T1 and T3 (Fig. 6a–c), which may be attributed to the azimuthal SVF_s feature of the pyranometer of T2, which was generally opposite to that of T1 and T3 (Fig. 7).

Another evidence arises from analyzing the interaction between terrain and sky condition. The effects of terrain on Q_p/R_s were greater on clear days than on overcast days, which was mainly attributed to the effect of terrain, since the effect is greater on direct solar beam than on diffuse radiation (Whiteman et al. 1989). The terrain effects also interacted with the meteorological factors. When the influence of solar zenith angle was excluded, the effects of terrain on Q_p/R_s were enhanced on clear days (Fig. 6g–l). Since the effects of terrain on redistribution of solar radiation are closely related to the geometric relationship between the sun position and the terrain, and the effects were partially masked when the solar zenith angle is low (Wang et al. 2006; Zhang et al. 2019). Differently, the terrain effects were weakened on clear days, when the influence of sky condition or water vapor pressure was excluded (Fig. 6j, k). Variations in Q_p/R_s are partly contributed by meteorological factors, and the terrain effect may be enhanced by the coupled interaction between meteorological factors and terrain factors. The performance of RF model improved when the terrain effect was included for prediction of Q_p/R_s (Fig. 8). This indicates that including terrain factors for the prediction of Q_p/R_s can improve the prediction accuracy. Moreover, we found that the importance of terrain effect increases as the sky condition changes from overcast to clear (Fig. 8), which is consistent with the expectations. In summary, the results suggest terrain can explain the observed variation in Q_p/R_s, indirectly supporting the finding that topography alters Q_p/R_s above the forest canopy.

Here, despite our efforts to explore the relationship between Q_p/R_s and complex terrain, there are still some limitations. First, we only used the sky view factor azimuthally corresponding to incidence solar radiation to represent the terrain feature, while the contribution of the other sectors of non-solar incidence azimuths was not included for analysis. Second, our analysis was based on field-observation, which cannot explain the mechanism of radiation-terrain interaction. For example, amount of solar radiation and its components reflected from the surrounding terrain cannot be quantified. Third, pyranometers were placed at a relatively high position to measure incoming solar radiation into the forest ecosystem. If the pyranometers are relocated to a low position, the influence of terrain on Q_p/R_s may strengthen, as the surrounding terrain and vegetation would exert a larger obstructing effect on the field of view of the pyranometer.

Conclusion

We validated the proposed hypothesis that topography alters Q_p/R_s above forest canopy through measurements of solar radiation and photosynthetic photon flux density at three sites in a valley. We found the significant differences in both daily and half-hour Q_p/R_s among the three sites, which were more pronounced on clear days than on overcast days. Q_p/R_s decreased with the increase of clearness index, while increased with water vapor pressure and the cosine of the solar zenith angle. Specially, the effects of water vapor pressure or solar zenith angle on Q_p/R_s were weakened when the influence of other meteorological factors was excluded, indicating that the effects of water vapor and solar incident path length on Q_p/R_s were not independent. Notably, sky view factor of sectors significantly influenced Q_p/R_s. Compared with using meteorological factors alone, the explanation of Q_p/R_s was improved when sky view factor was included in the predictor variables set, and the improvement in the explanatory power was greater on clear and partially cloudy days than on overcast days. These results imply that the surrounding terrain may affect Q_p/R_s. To develop accurate models for predicting Q_p/R_s in mountainous

areas, the influence of topography on Q_p/R_s should be investigated under various sky conditions.

Abbreviations

Q_p	Photosynthetic photon flux density
PAR	Photosynthetically active radiation
R_s	Global solar radiation
SVF_s	Sky view factor of sectors
FOV	Field of view
K_t	Clearness index
e	Water vapor pressure
cosθ	The cosine value of the solar zenith angle
T1	Tower 1
T2	Tower 2
T3	Tower 3

Supplementary Information

The online version contains supplementary material available at https://doi.org/10.1186/s13717-024-00514-8.

Additional file 1. Fig. S1. The diurnal variations of Q_p/R_s on overcast days in each month of the growing season (No suitable overcast days were found in October). **Fig. S2.** The diurnal variations of Q_p/R_s on clear days in each month of the growing season (No suitable clear days were found in August).

Acknowledgements
We thank Ting Zhang, Jing Wang, Jin Xie, Rong Li, and Junfeng Yuan from the Institute of Applied Ecology, Chinese Academy of Sciences for their suggestions on writing the manuscript.

Author contributions
Shuangtian Li: Investigation, Methodology, Software, Formal analysis, Writing—original draft. Qiaoling Yan: Conceptualization, Writing—review & editing, Funding acquisition, Supervision. Tian Gao: Investigation, Methodology, Funding acquisition, Writing—review & editing. Xingchang Wang: Methodology, Writing—review & editing. Qingwei Wang: Writing—review & editing. Fengyuan Yu: Investigation. Deliang Lu: Methodology. Huaqi Liu: Investigation. Jinxin Zhang: Supervision. Jiaojun Zhu: Conceptualization .

Funding
This research was supported by the National Key R&D Program of China (2016YFC0500300), the Strategic Leading Science & Technology Programme, CAS (XDA23070100) and National Natural Science Foundation of China (31870533).

Availability of data and materials
Please contact the author for data requests.

Declarations

Ethics approval and consent to participate
Not applicable.

Consent for publication
Not applicable.

Competing interests
The authors declare that they have no competing interests.

Author details
[1]CAS Key Laboratory of Forest Ecology and Silviculture, Institute of Applied Ecology, Chinese Academy of Sciences, Shenyang 110016, China, . [2]Qingyuan Forest CERN, National Observation and Research Station, Chinese Academy of Sciences, Shenyang 110016, China. [3]CAS-CSI Joint Laboratory of Research and Development for Monitoring Forest Fluxes of Trace Gases and Isotope Elements, Institute of Applied Ecology, Chinese Academy of Sciences (CAS), Shenyang 110016, China. [4]University of Chinese Academy of Sciences, Beijing 100049, China. [5]Center for Ecological Research, Northeast Forestry University, Harbin 150040, China.

Received: 24 January 2024 Accepted: 10 April 2024
Published online: 10 May 2024

References

Aguilar C, Herrero J, Polo MJ (2010) Topographic effects on solar radiation distribution in mountainous watersheds and their influence on reference evapotranspiration estimates at watershed scale. Hydrol Earth Syst Sci 14(12):2479–2494. https://doi.org/10.5194/hess-14-2479-2010

Akitsu T, Kume A, Hirose Y, Ijima O, Nasahara KN (2015) On the stability of radiometric ratios of photosynthetically active radiation to global solar radiation in Tsukuba, Japan. Agric For Meteorol 209:59–68. https://doi.org/10.1016/j.agrformet.2015.04.026

Akitsu T, Nasahara KN, Hirose Y, Ijima O, Kume A (2017) Quantum sensors for accurate and stable long-term photosynthetically active radiation observations. Agric For Meteorol 237:171–183. https://doi.org/10.1016/j.agrformet.2017.01.011

Akitsu T, Nasahara KN, Ijima O, Hirose Y, Ide R, Takagi K, Kume A (2022) The variability and seasonality in the ratio of photosynthetically active radiation to solar radiation: a simple empirical model of the ratio. Int J Appl Earth Obs 108:102724. https://doi.org/10.1016/j.jag.2022.102724

Alados I, Alados-Arboledas L (1999) Direct and diffuse photosynthetically active radiation: measurements and modelling. Agric For Meteorol 93(1):27–38. https://doi.org/10.1016/S0168-1923(98)00107-5

Alados I, Foyo-Moreno I, Alados-Arboledas L (1996) Photosynthetically active radiation: measurements and modeling. Agric For Meteorol 78:121–131. https://doi.org/10.1016/0168-1923(95)02245-7

Allen RG, Trezza R, Tasumi M (2006) Analytical integrated functions for daily solar radiation on slopes. Agric For Meteorol 139:55–73. https://doi.org/10.1016/j.agrformet.2006.05.012

Bosch JL, López G, Batlles FJ (2009) Global and direct photosynthetically active radiation parameterizations for clear-sky conditions. Agric For Meteorol 149(1):146–158. https://doi.org/10.1016/j.agrformet.2008.07.011

Breiman L (2001) Random forests. Mach Learn 45:5–32. https://doi.org/10.1023/a:1010933404324

Campbell GS, Norman JM (1998) An introduction to environmental biophysics, 2nd Edition, Springer Verlag, Berlin, Heidelberg, New York, pp. 286. https://doi.org/10.1016/S0176-1617(99)80035-2

Chen Q, Gao T, Zhu J, Wu F, Li X, Lu D, Yu F (2022) Individual tree segmentation and tree height estimation using leaf-off and leaf-on UAV-LiDAR data in dense deciduous forests. Remote Sens 14(12):2787. https://doi.org/10.3390/rs14122787

Dubayah R, Rich PM (1995) Topographic solar radiation models for GIS. Int J Geogr Inf Syst 9(4):405–419. https://doi.org/10.1080/02693799508902046

Foyo-Moreno I, Alados I, Alados-Arboledas L (2017) A new conventional regression model to estimate hourly photosynthetic photon flux density under all sky conditions. Int J Climatol 37:1067–1075. https://doi.org/10.1002/joc.5063

Gao T, Yu L, Yu F, Wang X, Yang K, Lu D, Li X, Yan Q, Sun Y, Liu L, Xu S, Zhen X, Ni Z, Zhang J, Wang G, Wei X, Zhou X, Zhu J (2020) Functions and applications of multi-tower platform of Qingyuan Forest Ecosystem Research Station of Chinese Academy of Sciences. Chin J Appl Ecol 31(3):695–705. https://doi.org/10.13287/j.1001-9332.202003.040

Ham JM (2005) Useful equations and tables in micrometeorology. In: Hatfield JL, Baker JM (eds) Micrometeorology in agricultural systems. American Society of Agronomy Inc., Madison, pp 533–560. https://doi.org/10.2134/agronmonogr47.c23

Hu B, Wang Y (2012) The climatological characteristics of photosynthetically active radiation in arid and semi-arid regions of China. J Atmos Chem 69:175–186. https://doi.org/10.1007/s10874-012-9235-4

Jacovides CP, Tymvios FS, Asimakopoulos DN, Theofilou KM, Pashiardes (2003) Global photosynthetically active radiation and its relationship with global solar radiation in the Eastern Mediterranean basin. Theor Appl Climatol 74:227–233. https://doi.org/10.1007/s00704-002-0685-5

Jacovides CP, Tymvios FS, Assimakopoulos VD, Kaltsounides NA (2007) The dependence of global and diffuse PAR radiation components on sky conditions at Athens, Greece. Agric For Meteorol 143(3–4):277–287. https://doi.org/10.1016/j.agrformet.2007.01.004

Li R, Zhao L, Ding Y, Wang S, Ji G, Xiao Y, Liu G, Sun L (2010) Monthly ratios of PAR to global solar radiation measured at northern Tibetan Plateau, China. Sol Energy 84(6):964–973. https://doi.org/10.1016/j.solener.2010.03.005

Li X, Zhang S, Chen Y (2016) Error assessment of grid-based diffuse solar radiation models. Int J Geogr Inf Sci 30(10):2032–2049. https://doi.org/10.1080/13658816.2016.1155215

Li Z, Li Z, Tong X, Zhang J, Dong L, Zheng Y, Ma W, Zhao L, Wang L, Wen L, Dang Z, Tuvshintogtokh I, Liang C, Li FY (2020) Climatic humidity mediates the strength of the species richness-biomass relationship on the Mongolian Plateau steppe. Sci Total Environ 718:137252. https://doi.org/10.1016/j.scitotenv.2020.137252

Mayer H, Holst T, Schindler D (2002) Microclimate within beech stands—part I: photosynthetically active radiation. Forstwiss Centralbl 121:301–321. https://doi.org/10.1046/j.1439-0337.2002.02038.x

McCree KJ (1972) Test of current definitions of photosynthetically active radiation against leaf photosynthesis data. Agric Meteorol 10:443–453. https://doi.org/10.1016/0002-1571(72)90045-3

Mizoguchi Y, Ohtani Y, Aoshima T, Hirakata A, Yuta S, Takanashi S, Iwata H, Nakai Y (2010) Comparison of the characteristics of five quantum sensors. Bull FFPRI 9:113–120

Papaioannou G, Nikolidakis G, Asimakopoulos D, Retalis D (1996) Photosynthetically active radiation in Athens. Agric For Meteorol 81(3–4):287–298. https://doi.org/10.1016/0168-1923(95)02290-2

Proutsos N, Liakatas A, Alexandris S (2019) Ratio of photosynthetically active to total incoming radiation above a Mediterranean deciduous oak forest. Theor Appl Climatol 137:2927–2939. https://doi.org/10.1007/s00704-019-02786-z

Qin W, Wang L, Lin A, Zhang M, Xia X, Hu B, Niu Z (2018) Comparison of deterministic and data-driven models for solar radiation estimation in China. Renew Sust Energ Rev 81:579–594. https://doi.org/10.1016/j.rser.2017.08.037

Tetens O (1930) Uber einige meteorologische Begriffe. Z Geophys 6:297–309

Tsubo M, Walker S (2005) Relationships between photosynthetically active radiation and clearness index at Bloemfontein, South Africa. Theor Appl Climatol 80:17–25. https://doi.org/10.1007/s00704-004-0080-5

Wang Q, Tenhunen J, Schmidt M, Otieno D, Kolcun O, Droesler M (2005) Diffuse PAR irradiance under clear skies in complex alpine terrain. Agric For Meteorol 128(1–2):1–15. https://doi.org/10.1016/j.agrformet.2004.09.004

Wang Q, Tenhunen J, Schmidt M, Kolcun O, Droesler M, Reichstein M (2006) Estimation of total, direct and diffuse PAR under clear skies in complex alpine terrain of the National Park Berchtesgaden, Germany. Ecol Model 196(1–2):149–162. https://doi.org/10.1016/j.ecolmodel.2006.02.005

Wang L, Gong W, Ma Y, Hu B, Zhang M (2014) Photosynthetically active radiation and its relationship with global solar radiation in Central China. Int J Biometeorol 58:1265–1277. https://doi.org/10.1007/s00484-013-0690-7

Wang L, Gong W, Hu B, Lin A, Li H, Zou L (2015a) Modeling and analysis of the spatiotemporal variations of photosynthetically active radiation in China during 1961–2012. Renew Sust Energ Rev 49:1019–1032. https://doi.org/10.1016/j.rser.2015.04.174

Wang L, Gong W, Hu B, Zhu Z (2015b) Analysis of photosynthetically active radiation in Northwest China from observation and estimation. Int J Biometeorol 59:193–204. https://doi.org/10.1007/s00484-014-0835-3

Whiteman CD, Allwine KJ, Fritschen LJ, Orgill MM, Simpson JR (1989) Deep valley radiation and surface energy budget microclimates. Part I: radiation. J Appl Meteorol 28(6):414–426. https://doi.org/10.1175/1520-0450(1989)028%3c0414:DVRASE%3e2.0.CO;2

Yamashita M, Yoshimura M (2019) Estimation of global and diffuse photosynthetic photon flux density under various sky conditions using ground-based whole-sky images. Remote Sens 11(8):932. https://doi.org/10.3390/rs11080932

Yu X, Wu Z, Jiang W, Guo X (2015) Predicting daily photosynthetically active radiation from global solar radiation in the Contiguous United States. Energ Convers Manage 89:71–82. https://doi.org/10.1016/j.enconman.2014.09.038

Zhang S, Li X, She J, Peng X (2019) Assimilating remote sensing data into GIS-based all sky solar radiation modeling for mountain terrain. Remote Sens Environ 231:111239. https://doi.org/10.1016/j.rse.2019.111239

Zhu Z, Wang L, Gong W, Xiong Y, Hu B (2015) Observation and estimation of photosynthetic photon flux density in Southern China. Theor Appl Climatol 120:701–712. https://doi.org/10.1007/s00704-014-1204-1

Publisher's Note